Available online at www.sciencedirect.com

ScienceDirect

MATTER AND RADIATION AT EXTREMES

Matter and Radiation at Extremes 2 (2017) 263–274

www.journals.elsevier.com/matter-and-radiation-at-extremes

Research Article

Formation of Field Reversed Configuration (FRC) on the Yingguang-I device

Qizhi Sun [a,b], Xianjun Yang [c], Yuesong Jia [a,b,*], Lulu Li [c], Dongfan Fang [a,b], Xiaoming Zhao [a,b], Weidong Qin [a,b], Zhengfen Liu [a,b], Wei Liu [a,b], Jun Li [a,b], Yuan Chi [a,b], Xiaoguang Wang [c]

[a] *Institute of Fluid Physics, China Academy of Engineering Physics, Miangyang 621900, China*
[b] *Key Laboratory of Pulsed Power Technology and Science, China Academy of Engineering Physics, Miangyang 621900, China*
[c] *Institute of Applied Physics and Computational Mathematics, Beijing 100088, China*

Received 17 July 2016; revised 24 May 2017; accepted 18 July 2017
Available online 18 August 2017

Abstract

As a hybrid approach to realizing fusion energy, Magnetized Target Fusion (MTF) based on the Field Reversed Configuration (FRC), which has the plasma density and confinement time in the range between magnetic and inertial confinement fusion, has been recently widely pursued around the world. To investigate the formation and confinement of the FRC plasma injector for MTF, the Yingguang-I, which is an FRC test device and contains a multi-bank program-discharged pulsed power sub-system, was constructed at the Institute of Fluid Physics (IFP), China. This paper presents the pulsed power components and their parameters of the device in detail, then gives a brief description of progress in experiments of FRC formation. Experimental results of the pulsed power sub-system show that the peak current/magnetic field of 110 kA/0.3 T, 10 kA/1.2 T and 1.7 MA/3.4 T were achieved in the bias, mirror and θ-pinch circuits with quarter cycle of 80 μs, 700 μs and 3.8 μs respectively. The induced electric field in the neutral gas was greater than 0.25 kV/cm when the ionization bank was charged to 70 kV. With H_2 gas of 8 Pa, the plasma target of density 10^{16} cm^{-3}, separatrix radius 4 cm, half-length 17 cm, equilibrium temperature 200 eV and lifetime 3 μs (approximately the half pulse width of the reversed field) have been obtained through the θ-pinch method when the bias, mirror, ionization and θ-pinch banks were charged to 5 kV, 5 kV, 55 kV and ±45 kV respectively. The images from the high-speed end-on framing camera demonstrate the formation processes of FRC and some features agree well with the results with the two-dimension magneto hydrodynamics code (2D-MHD).

PACS codes: 84.70.+p; 52.55.Lf; 52.25.Xz

Keywords: Magnetized Target Fusion (MTF); Field Reversed Configuration (FRC); Magnetized plasma; Pulsed power

1. Introduction

In the past several decades, the controlled fusion programs have concentrated on magnetic confinement fusion (MCF, typical device is ITER) and inertial confinement fusion (ICF, typical device is NIF). MCF is of lower plasma density and longer confinement time, while ICF, on the contrary, is of higher density and shorter confinement time. Magnetized Target Fusion (MTF) which usually employs the Field Reversed Configuration (FRC) with the moderate plasma density and confinement time is a hybrid approach to fusion energy. Compared to the traditional fusion research, MTF has some distinguishing features. (1) Parameters of MTF plasma are moderate. Usually the density and energy confinement time of MCF are about 10^{14} cm^{-3} and several or more seconds respectively [1], while ICF density might be as high as

* Corresponding author. Institute of Fluid Physics, China Academy of Engineering Physics, Miangyang 621900, China.
E-mail address: jysniper@163.com (Y.S. Jia).
Peer review under responsibility of Science and Technology Information Center, China Academy of Engineering Physics.

http://dx.doi.org/10.1016/j.mre.2017.07.003

10^{26} cm^{-3} and its fusion burn time be as short as a few nanoseconds [2]. However, MTF with the plasma density of 10^{20} cm^{-3} and the confinement time of several to hundreds of microseconds would make the fusion system more compact [3,4]. (2) Moderate parameters, especially the time scale of microsecond for fusion enable low-cost construction of the pulsed power device. The cost of ITER and NIF are nearly ten billion dollars. However, it's only several hundred million dollars for MTF. That's why more and more investors choose MTF on their way to fusion. (3) High β (plasma pressure/magnetic field pressure) value of FRC plasma results in high-power density of fusion energy according to the scaling law $P/V \sim \beta^2 B^4$, where P, V, B are the fusion power, the plasma volume and the magnetic field respectively. This merit results from that the magnetic field in the core of plasma is relatively small [5], and the FRC target is a self-organized (SO) plasma.

As the best studied plasma target for MTF, FRC also has some other distinguishing properties claimed by Steinhauer [5] and Tuszewski [6]. (1) Wall separation: the FRC plasma is highly isolated from the wall by the magnetic field in vacuum region, and the separation distance is generally 2–3 times of the FRC target radius in experiments. The wall separation makes the FRC plasma less vulnerable to impurity and thermal loss. (2) Little or no toroidal field: simple magnetic field structure with no toroidal field coils may eliminate the specter of magnetic surface disruption (which is a serious problem in MCF). (3) Movability: the FRC can be formed in an independent chamber and translated into a separate confinement chamber, and it's more suitable for compression.

Due to FRCs' advantages in fusion program as mentioned above, many devices have been built around the world to investigate the FRC plasma formation, confinement, translation and compression. Based on the theta (θ)-pinch method, a series of devices named as FRX-A [7], FRX-B [8], FRX-C [9] and FRX-L [10] have been built in Los Alamos National Laboratory (LANL). On these devices, the formation, confinement, sustainment and translation of a high density and high temperature FRC plasma were studied respectively. The typical D-T plasma target with density of 10^{16} cm^{-3}, equilibrium temperature of 200–700 eV and plasma radius of 1.5–2.5 cm has been achieved on the FRX-L. Since 2008 [11] a team led by LANL and the Air Force Research Laboratory (AFRL) has been investigating solid liner compression of FRC plasmas to achieve keV temperatures on the FRCHX device [12] of which the FRX-L acts as the plasma injector and the Shiva Star as the plasma compressor. Also, adopting the θ-pinch method the plasma density is about 10^{15} cm^{-3}, temperature is 200–300 eV and the plasma radius is 5–7 cm on the NUCTE-III device [13] in Nihon University. Merging-spheromak is another method for FRC formation just like that adopted in TS-3 [14], TS-4 [15] and MRX [16] devices with the typical plasma density of 10^{14} cm^{-3}, temperature of 10–100 eV and plasma radius of 20–70 cm. Based on the collision-merging method the C-2 [17,32] device constructed in Tri Alpha Energy (TAE) has proved the high performance of FRC plasma with the confinement time of several milliseconds [18]. According to the proposal of Direct Fusion Drive (DFD), a series of PFRC (Princeton Field Reversed Configuration) devices have been constructed by Princeton Satellite Systems (PSS) and Princeton Plasma Physics Laboratory (PPPL) to investigate the FRC fusion reactor which can provide the power and propulsion in deep space travel [19]. The FRC physics also has been studied on other devices such as TCS [20], TCS-U [21], Colorado [22] and IFRC [23].

To investigate the formation and confinement of the FRC plasma injector for the MTF, Yingguang-I, driven by a multi-bank program-discharged pulsed power system was designed in 2013 [24]. Yingguang-I device was constructed at the Institute of Fluid Physics, Chinese Academy of Engineering Physics (CAEP). In this paper, we will focus on the development of Yingguang-I device and the formation of FRC plasma on this device. In Sec. II, we will present the pulsed power components and their parameters in detail. In Sec. III, we will briefly describe the experimental results of the gas ionization on this device. In Sec. IV, we will demonstrate the formation of FRC and present the main experimental results. In Sec. V we will give a summary and describe the future work on this device.

2. Development of the Yingguang-I device

In MTF there are usually three distinct steps (shown in Fig. 1) named as the FRC formation, translation and compression respectively [25]. Firstly, the pre-heated FRC target is formed in the formation zone in a quartz tube, then the target ejects out by the gradient magnetic field through the translation zone and is captured by the end-on mirror coils in the compression zone. Finally, a large mass liner compresses the FRC target adiabatically to fusion ignition conditions. There are many kinds of approaches to the FRC formation such as the rotating magnetic field method employed at University of Washington [26] and University of Princeton [26], collision-merging at Tri Alpha Energy [28] and θ-pinch at LANL [29], and plasma gun at General Fusion [27]. Furthermore, the pusher for FRC compression could be the metal solid liner adopted by LANL [28], the liquid metal by General Fusion [29], or the plasma liner in Hyper-V [30].

Generally, FRC is characterized by the closed-field-line topology (shown in Fig. 2) and belongs to the compact toroid (CT) family of magnetized plasmas. To form a pre-heated FRC target by the θ-pinch method, there are 5 steps shown in Fig. 3. A) Biasing: the mirror and bias capacitor banks are discharged in sequence (see Fig. 4) to create a magnetic field (called the bias field) in the neutral gas. B) Ionization: the ionization bank is then discharged to produce a

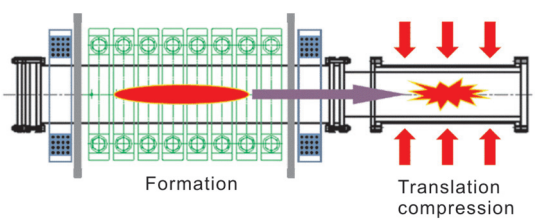

Fig. 1. Three steps in MTF.

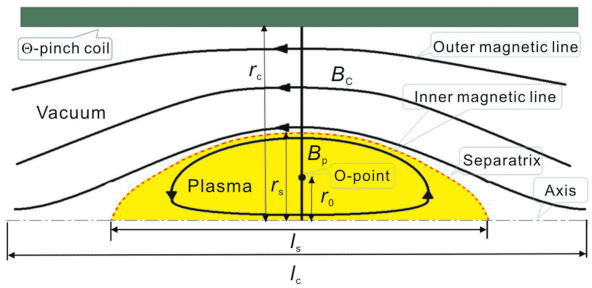

Fig. 2. Sketch of FRC plasma target.

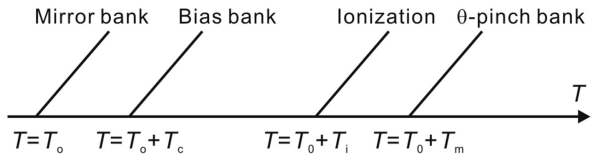

Fig. 4. Programmed discharging sequence for FRC formation.

plasma in the quartz tube by the induced electric field and the bias field is frozen with the plasma. C) Reversing: the θ-pinch bank is discharged to produce a reversed magnetic field outside the plasma which will compress the plasma radially. D) Reconnection: when the reversed field diffuses into the plasma, the magnetic line reconnects with the frozen bias field line at the near end of the mirror coils. E) Equilibrium: after the magnetic field line reconnection, the plasma shrinks axially due to the magnetic force. While the plasma equilibrates axially and radially the FRC target is formed. The FRC formation is a very important step in the MTF scheme because it produces a key effect on the plasma density, temperature, lifetime and other parameters.

In fact, the MTF based on FRC is a member of the so-called Magneto-Inertial Fusion (MIF) family of fusion approaches. Taking advantages of the magnetic confinement and inertial compression MIF could possibly operate efficiently. Besides the FRCHX device at Air Force Research Laboratory (AFRL) [31], several other facilities for the integrated MIF experiments such as MagLIF (Magnetized Liner Inertial Fusion) at Sandia National Laboratory [33] and Acoustically Driven (AD) MTF at General Fusion Company [34] have been developed. Yingguang-I device was constructed to investigate the formation and confinement of the FRC plasma injector for the MTF. Unlike the rotating magnetic field method on TCS (Translation Confinement Sustainment) device at University of Washington, and the plasma gun on AD at General Fusion company, the formation method on Yingguang-I device is based on the field reversed θ-pinch (FRTP), just like that on C-2 device at Tri Alpha Energy company and FRX-L at LANL. Besides the formation of high temperature and high density FRC plasma target, Yingguang-I device can also be used to study the collisionless shocks, the magnetic reconnection and plasma propulsion. As a microsecond pulse power device, Yingguang-I consists of multi-bank pulsed power systems, time controlling and trigger system, FRC formation coils and diagnostics. The components and parameters of the banks for mirror, bias, ionization and θ-pinch are listed in Table 1 and shown in Fig. 5. Some photos of the Yingguang-I device are shown in Fig. 6.

The mirror bank connects with the mirror coils through eight cables independently and the bias, ionization and θ-pinch banks are discharged in parallel to the same load (θ-pinch coil). Precise trigger sequence of these three banks is necessary for the formation of plasma target. The bias bank, with a quarter cycle of $t_{1/4} = 80$ μs and maximum current 110 kA, is triggered at first to produce a slowly varying field which later makes the plasma magnetized. Upon reaching the peak of the bias field, the ionization bank is triggered, with

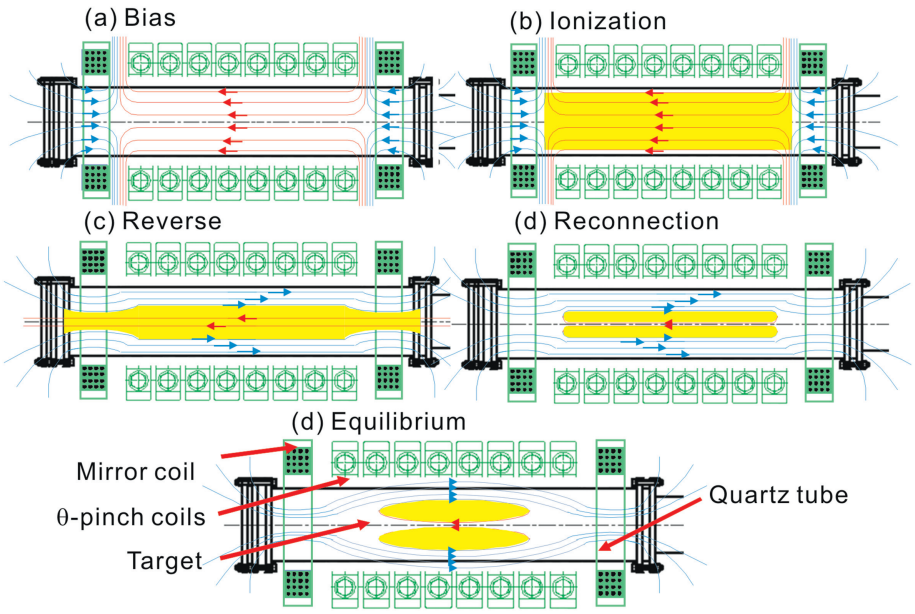

Fig. 3. Physical processes of FRC formation.

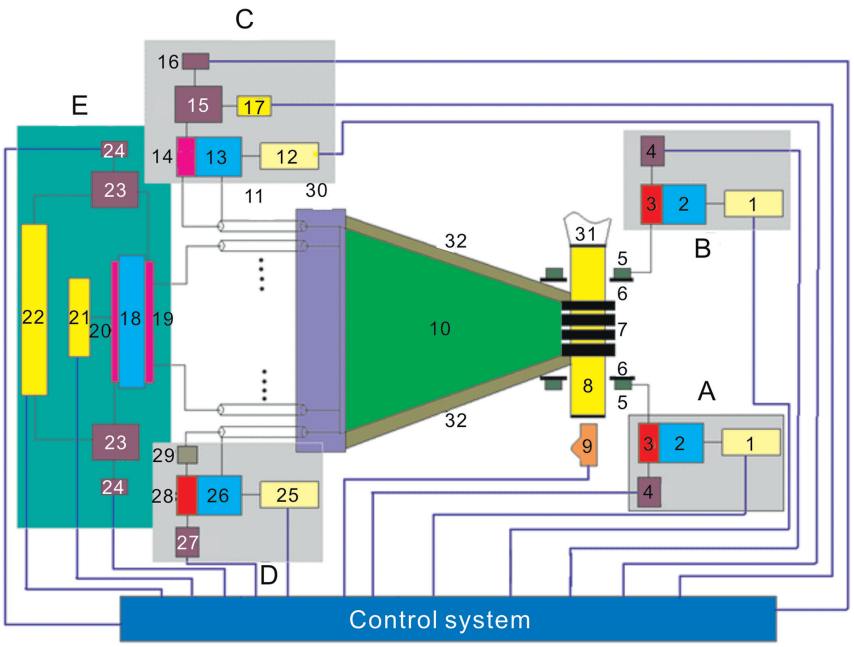

Fig. 5. Circuit topology of Yingguang-I device. A, B- pulsed power system of mirror coils; C- ionization bank system; D- bias bank system; E- θ-pinch bank system. 1-power source (10 kV/0.6 A); 2-capacitor bank (2 mF/10 kV); 3-ignitron switch (NL-8900); 4-ignitron trigger; 5-mirror coil (~164 μH); 6-flux isolated plane; 7-θ-pinch coils (eight in parallel); 8-quartz tube with the working gas; 9-high speed framing camera; 10-flat transmission line; 11-transmission cable (64 in parallel); 12-power source (100 kV/60 mA); 13-ionization bank (3 μF/100 kV); 14-rail gap switch; 15-four-staged Marx as the trigger (200 kV/20 ns); 16-high voltage source (15–20 kV); 17-power source (±50 kV/150 mA); 18-θ-pinch bank (±100 kV/2 × 72 μF); 19-crowbar switch (6 in parallel); 20-closing switch (6 in parallel); 21-power source (±100 kV/60 mA); 22-power source (±50 kV/150 mA); 23-four-staged Marx as the trigger (200 kV/20 ns); 24-high voltage source (15–20 kV); 25-power source (10 kV/0.6 A); 26-bias bank (2 mF/10 kV); 27-ignitron trigger; 28-ignitron switch (NL-8900); 29-isolated inductor (4 μH); 30-insulation box; 31-vacuum system (10^{-5} Pa); 32-insulation layer.

$t_{1/4} = 3$ μs and maximum current 400 kA. This fast oscillating field ionizes the neutral gas completely by the processes similar to those occurring in Inductively Coupled Discharge (ICD). Once the ionization process is completed, the bias field lines are frozen inside the plasma, and the θ-pinch bank with a quarter cycle $t_{1/4} = 3.8$ μs and maximum current 1.7 MA is triggered to generate a reversed field whose direction is opposite to the bias field, and magnitude is 10 times larger than that of the bias field. As a result of the strong magnetic pressure, the plasma begins to contract radially and the field lines reconnect near the end region of the mirror coils which symbolize the closed-field-line topology in the formed plasma. According to the discharged parameters and the gas ionization conditions, we chose the trigger timing sequence as T_0 ~50 μs, $T_0 + T_c$ ~ 480 μs, $T_0 + T_I$ ~ 540 μs, $T_0 + T_m$ ~ 568 μs for the mirror, bias, ionization and θ-pinch banks respectively. The discharged parameters of the banks are listed in Table 2 and typical waveform are shown in Fig. 7.

The key unit of Yingguang-I device are undoubtedly the high-current rail gap switches and its trigger system.

Fig. 8 shows the design configuration, the photo and the operation space of the rail gap switch when the mixture of 25% SF_6 and 75% N_2 is adopted as the insulation gas. Utilizing the casted base with the copper electric connection makes the gas sealing simpler and the mechanical strength higher. As the test platform with 9 μF capacitor bank was charged to 70 kV, and the gap was set to 2 cm, a peak current of 400 kA, an electric charge of more than 10 C, and a discharge channel number of greater than 5 were achieved in the experiments. Although the switch was not destroyed by electromagnetic force in this particular test, the operating current of the rail gap switch has been limited to 250 kA in the Yingguang-I device on consideration of reliable operation of the device. After running 200 times, we must clean the electrode and the base to avoid unexpected breakdown from the pollution during its discharge.

Table 1
Components and parameters of banks for mirror, bias, ionization and θ-pinch.

	Bias	Mirror	Ionization	θ-pinch
Power source	20 kV/2.4 A	20 kV/2.4 A	100 kV/60 mA	±100 kV/200 mA
Capacitor bank	2 × 16 × 50 μF/20 kV	2 × 16 × 50 μF/20 kV 2 in parallel	3 × 3 μF/100 kV	2 × 4 × 3 μF/100 kV 6 in parallel
Switch	2 ignitron switches	4 ignitron switches	1 rail gap switch	6 rail gap switches
Trigger voltage	4 kV	4 kV	200 kV	200 kV

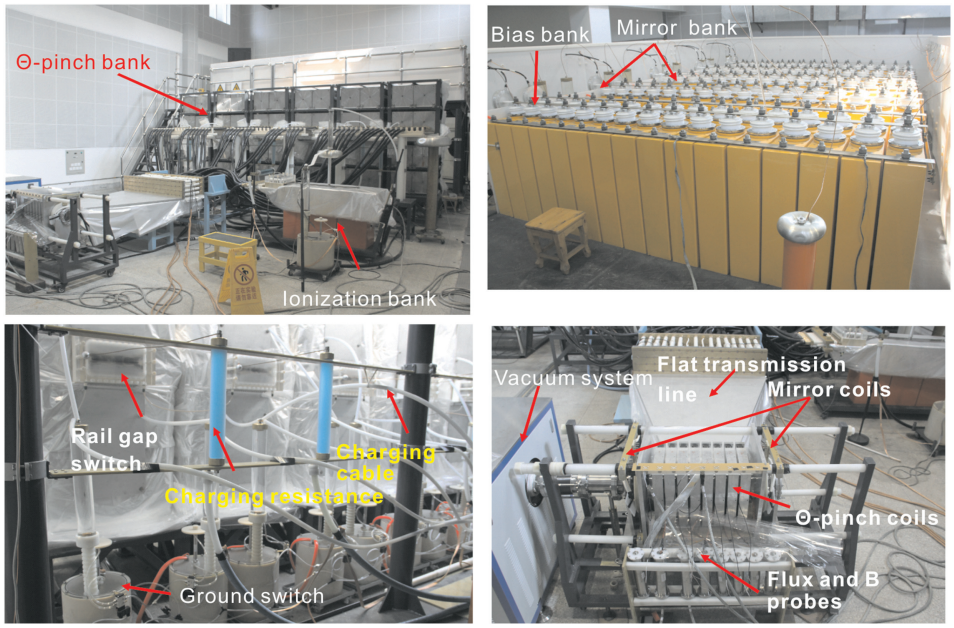

Fig. 6. Photos of the Yingguang-I device.

Table 2
Discharging parameters.

	Bias	Mirror	Ionization	θ-pinch
Charging voltage	7 kV	7 kV	70 kV	±60 kV
Inductance of circuit	1.6 μH	13 μH	350 nH	110 nH
Inductance of load	50 nH	170 μH	50 nH	50 nH
Quarter cycle (T/4)	~80 μs	~700 μs	~3 μs	~3.8 μs
Peak current	110 kA	10 kA	400 kA	1.7 MA
Peak field	0.3 T	1.2 T	0.25 kV/cm	3.4 T

The one rail gap switch in ionization bank and the six switches in the θ-pinch bank are triggered by the same two compact generators respectively. Fig. 9 shows the circuit (Fig. 9(a)) and the photo (Fig. 9(b)) of the trigger generator which consists of the trigger Marx, the three-staged main Marx and the sharp circuit. As the high voltage of 15–20 kV from t_r input, the trigger Marx was firstly fired and produced about 60 kV to initiate simultaneously the three-staged main Marx. By this method, we can enhance the reliability and repeatability of the trigger system. Sharp circuit connected to the end of the main Marx is used to decrease the rise time of the output voltage. When the charging voltage was set as ±30 kV, this generator produced a high voltage of over 200 kV with the rise time of less than 20 ns. The repeated tests shown in Fig. 9(c) confirm that the offset of start-up time is less than 100 ns. It's enough for good operation of the microsecond pulsed power device same as Yingguang-I device.

The diagnostics utilized in Yingguang-I device tests are summarized in Table 3 and illustrated in Fig. 10. The magnetic field probes (B probes) and flux probes array placed in the radial gap between the discharge quartz tube and the θ-pinch coil are used to measure the excluded magnetic field and excluded flux as a function of time. Separatrix radius can also be obtained in terms of the measured quantities by the following formula

$$r_s = r_c \cdot \sqrt{1 - \frac{\Phi_p}{\Phi_v}\frac{B_v}{B_p}}, \tag{1}$$

where r_s is the separatrix radius, r_c is the θ-pinch coil radius, Φ_p and B_p are measured by the flux and B probes respectively

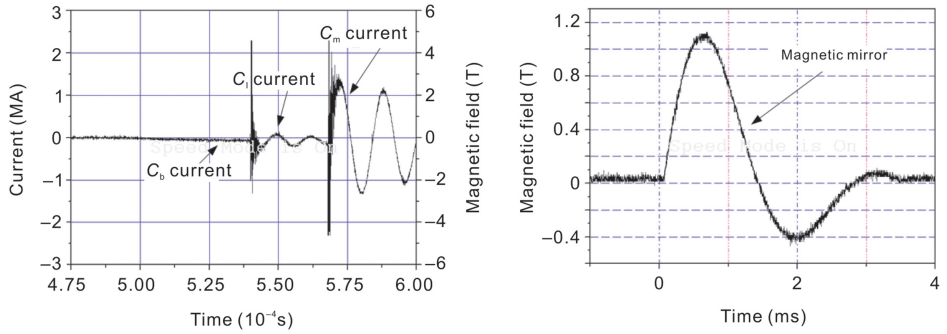

Fig. 7. Typical waveforms. C_b-the bias with charged voltage of 5 kV, C_I-the ionization with 55 kV, C_m-the θ-pinch with ±55 kV. Mirror bank was also charged to 5 kV.

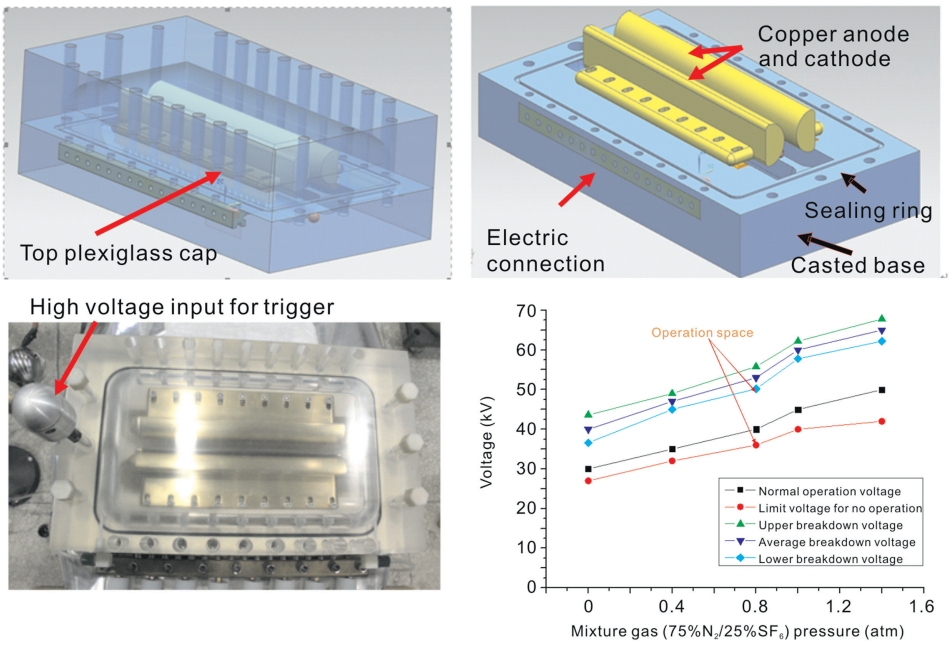

Fig. 8. Configuration, photo and operation space of the rail gap switch.

in the experiments with plasma and are related as $\Phi_p = B_p\pi\left(r_c^2 - r_s^2\right)$, and the Φ_v, B_v are measured in vacuum experiments without plasma and are related as $\Phi_v = B_v\pi r_c^2$. The single-chord laser interferometer with 630 nm wave length at the mid-plane of the quartz tube provides the average electron density as a function of time. Signals from the B probes, flux probes, and interferometer are recorded by oscilloscope with the maximum sampling rate of 1 GHz. Another important diagnostic is a high-speed multi-frame camera. Its resolution is 1600 × 1200 with the maximum of 200 million frames per second. In preliminary experiments, the camera is located at the end of quartz tube and can provide eight axial integrated self-luminescence images. A multiple-chord interferometer [35] which can provide the density distribution of the plasma with tomographic analysis, and also a laser shadow imaging camera for more distinguishable pictures than that shown in Fig. 10 are under development.

3. Gas ionization

Ionization will produce a magnetized plasma with the bias field before the θ-pinch bank is triggered. On Yingguang-I device, the ionization processes are the same as the traditional inductively coupled discharge (ICD) with a high current of 150–400 kA and frequency of 83 kHz passing through the θ-pinch coils. The basic steps of ionization are as the following: A) fast-rising current inductively generates a strong toroidal electric field around the circumference. B) Toroidal electric field firstly ionize the neutral gas near the surface of the quartz tube to form a plasma ring. C) On the basis of snowplow method, the inner neutral gas will be continuously ionized when the plasma ring driven by the Lorentz force moves inward. D) By the high frequency current the plasma ring oscillates radially and the inner gas would be ionized completely after 2–3 oscillations. During this process, the plasma temperature will also keep an oscillating increase and that's why we usually trigger the θ-pinch bank after 2–3 ionization periods.

To explore the reliability and stability of gas ionization on the Yingguang-1 device, the repetitive experiments of argon (Ar) gas are carried out with the bias magnetic field of 0.3 T (corresponding to charging voltage of 7 kV) and the gas pressure of 8 Pa. The induced maximum electric field of 0.16 kV/cm has been probed when the ionization bank was charged to 45 kV. In these experiments, we chose the trigger timing sequence as $T_0 \sim 20$ μs, $T_0 + T_I \sim 83$ μs for the bias and ionization banks respectively. The images from the end-on framing camera in a period of 12 μs are shown in Fig. 11 in which the interval between each image is about 1.5 μs. At the time of 83 μs, the ionization bank was triggered and the first image was recorded at 84.5 μs. The images from Fig. 11 illuminate that the ionization processes of Ar gas (from shot #1 to shot #6) behave repetitively. Fig. 12 shows the line integrated electron density obtained from the single-chord laser interferometer and the corresponding current/field curves. From Figs. 11 and 12 we can observe the oscillation processes of the plasma ring and the oscillating increase of the self-luminescence strength from plasma which can represents the plasma temperature. After the first period of discharged current, the electron density reaches a peak value about 5.3×10^{16} cm^{-2}. The peak of the electron density also appears periodically which may be resulted from the constriction and expansion of the plasma ring as the discharging current varies periodically.

When the plasma ring driven by the ionization field moves inward, the bias magnetic field will impose an opposite force

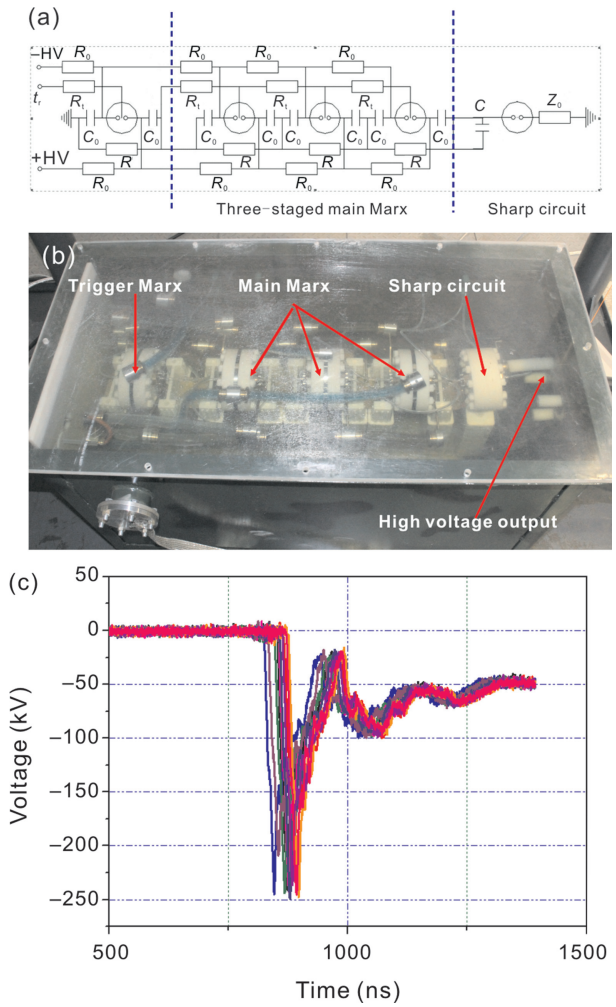

Fig. 9. (a) Circuit of the 200 kV/20 ns trigger generator. C_0-50 kV/0.1 μF, C-200 kV/70 nF; R_0, R, R_t-the charging, grounding and the triggering resistance respectively; Z_0-the output equivalent impedance of the generator; HV ± 50 kV power source; t_r- high voltage source (15–20 kV) to fire the first trigger Marx. (b) Photo of the 200 kV/20 ns trigger generator. (c) Repetitive test of the trigger generator.

on the ring and subsequently slowdown its movement. Meanwhile the frozen bias field can inhibit the collisional ionization between the electron and the neutral atom and result in the suppression of the gas ionization. Also, increase of bias field limits electron's gyration trajectory and deters ionization. To study the effect of bias field on the ionization, especially to find the suitable initial conditions under which the gas can be ionized completely, a series of contrast experiments on the Yingguang-I device have been executed with the bias field of 0.04 T, 0.1 T, 0.2 T and 0.3 T respectively. The ionization current/field is the same as that in Figs. 11 and 12. The images

Table 3
Diagnostics on Yingguang-I device.

Diagnostic device	Information
B & Flux probes array	Total flux; Average magnetic field; Magnetic field; Separatrix radius
Laser interferometer side-on	Average electron density; Areal density
Framing camera end-on	Plasma geometry and symmetry

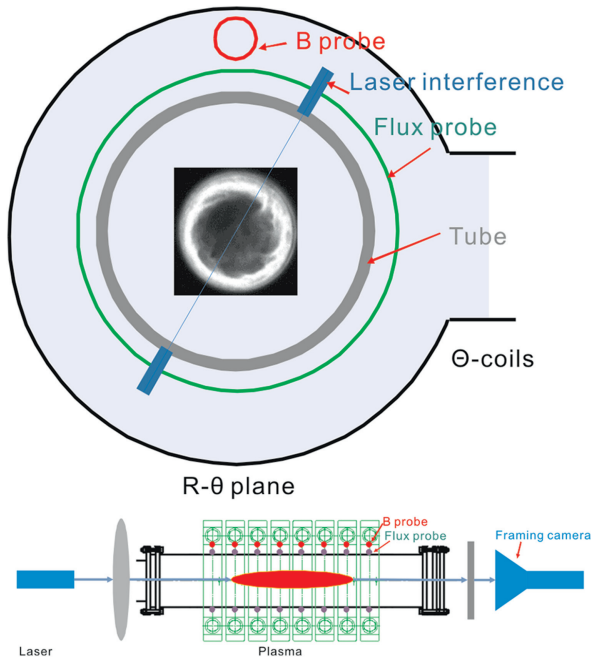

Fig. 10. Schematic of the diagnosis on the Yingguang-I device from end-on (up) and side-on (down).

during the first ionization period from the end-on framing camera are shown in Fig. 13. From Fig. 13 we can observe that with increase of bias magnetic field the inner radius of lighting ring becomes larger while the ring width becomes smaller at the same time. The self-luminance of the ring appears weaker and weaker as the bias field increases until there's no luminance. These experimental results show that the bias magnetic field not only can suppress the gas ionization but also can inhibit the increase of the plasma temperature during the stage of gas ionization.

The line integrated electron density from the single-chord laser interferometer can supply more detailed information to verify again that the bias field suppresses the gas ionization. Fig. 14 shows the line integrated electron density and the first peak value time with different bias magnetic field. In Fig. 14 the electron density refers to the first peak value while the peak value time means the time interval from the trigger time of the ionization bank to the first peak value of the electron density just seen in Fig. 12. The triangles indicate scattered experimental points and the fitting curve refers to the averaging value by statistical method. Although there are some dispersions especially at the bias field of 0.13 T (corresponding to charging voltage of 3 kV), we can find from Fig. 14 that the first peak value time increases and the maximum of electron density decreases with the bias magnetic field increases. That is to say the higher bias field the harder to ionize. From Fig. 14 we can also confirm that the bias field not greater than 0.21 T (corresponding to charging voltage of 5 kV) for hydrogen and 0.30 T (corresponding to charging voltage of 7 kV) for argon are good choices for complete ionizations in the case of ionization bank charging voltage of 45 kV and the gas pressure of 8 Pa.

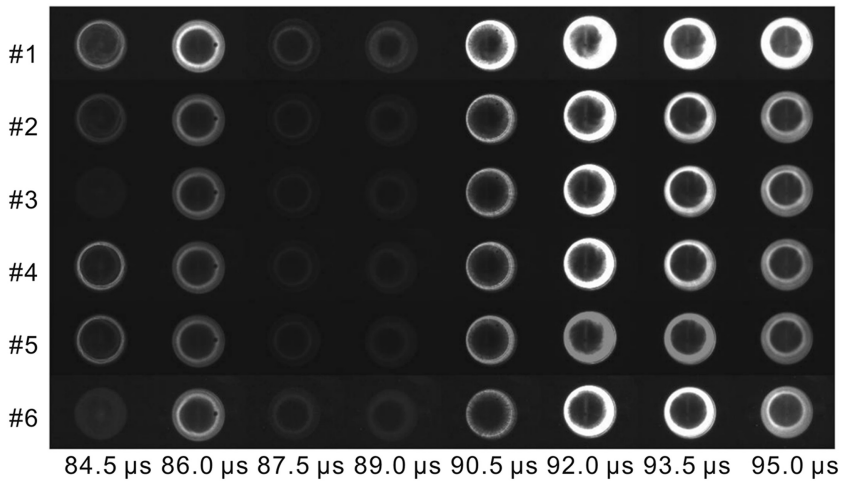

Fig. 11. Repeated experiments of ionization. Total 6 shots with 8 images for each, and the period of ionization is 12 μs, the exposure time of the camera was set as 50 ns.

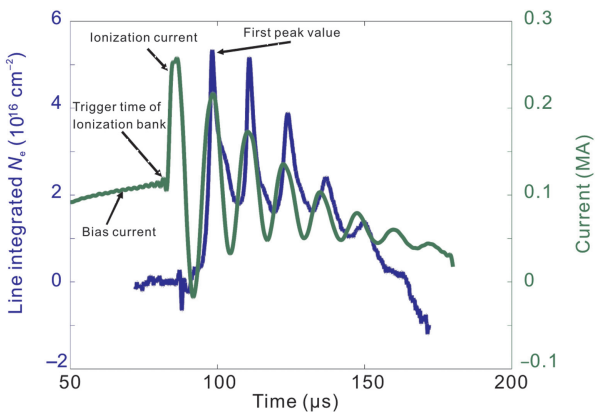

Fig. 12. Line integrated electron density from the single-chord laser interferometer and the corresponding current waveform.

4. FRC formation

Stable, reliable and robust formation of FRC plays an important role in MTF. Verification of the physical processes of the FRC formation is a prior task on Yingguang-I device. The typical current/magnetic field waveform and the images from the end-on framing camera are shown in Fig. 10 in which the mirror, bias, ionization and θ-pinch banks are charged to 5 kV, 5 kV, 45 kV and ±45 kV respectively. The corresponding field is 0.9 T, 0.2 T, 0.16 kV/cm and 2.6 T. Ar with the pressure of 8 Pa was filled initially in quartz tube. Fig. 15(a) shows the discharging sequence of the bias, ionization and the θ-pinch banks, and the vertical black line in Fig. 15(b) denotes the start-time of the framing camera with the time interval of 500 ns. From Fig. 15(c) we find that, after the ionization recorded in the former four images (marked by the yellow box) the θ-pinch bank was triggered, and then the plasma ring was accelerated inward by the strong magnetic pressure, and the self-luminance of the plasma ring that could be regarded as the plasma temperature increased quickly. When the reversed magnetic field diffused into plasma, a bright torus was formed at the outside surface of the target recorded in the following eight images (marked by the red box). At the peak of magnetic field the plasma torus came to the smallest radius and brightest luminance. After the peak field, the plasma dissipated gradually recorded in the rear six images (marked by the green box). The lifetime of FRC is about 3 μs (from 571 μs to 574 μs) approximately equals to the half pulse width of the θ-pinch field. In near future, we can prolong the lifetime of the FRC target on the Yingguang-I device by increasing the half pulse width of the θ-pinch field with the crowbar switch. The

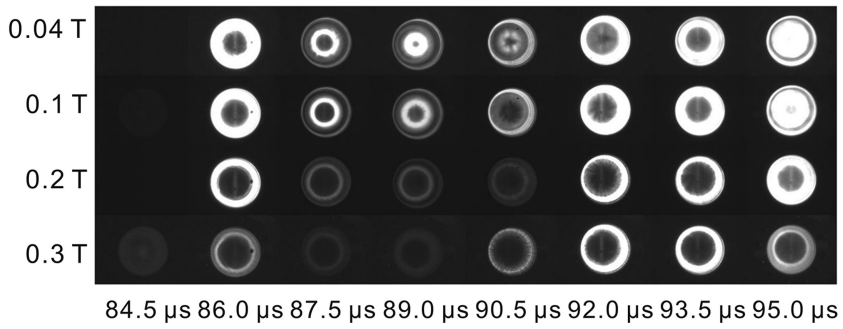

Fig. 13. Images from the end-on camera with the exposure time of 20 ns during first period of ionization with different bias magnetic field.

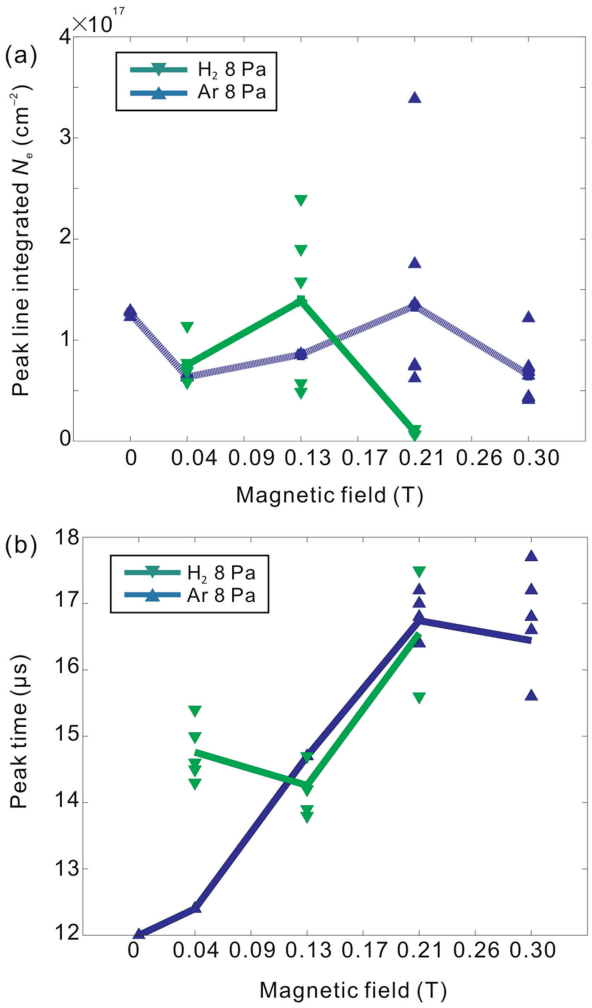

Fig. 14. Line integrated electron density and first peak value time with different bias magnetic field. (a) Dependency of electron density on the bias field. (b) Dependency of peak value time on the bias field.

magnetic line reconnection near the mirror coils should also be measured to verify the magnetic topology directly in future.

An MHD code named as MPF-2D developed by the Institute of Applied Physics and Computational Mathematics (IAPCM) [36–38] was used to simulate the formation processes of the FRC target. In MPF-2D simulation the gas was assumed to be fully ionized initially and the initial density was set to 2×10^{15} cm^{-3} which corresponds to 8 Pa hydrogen filled in quartz tube. Magnetic fields of mirror, bias and θ-pinch were set to 0.9 T, 0.2 T and 2.6 T respectively, which are the same as those in experiments. The comparison of separatrix radii between simulation and experimental data are plotted in Fig. 16(a). The experimental data are from shot 150910-01, 150910-02, 150911-02 and 150911-03. The separatrix radii of each shot were measured from images taken from high-speed multi-frame camera. The blue dashed line refers to calculated separatrix radius, which is defined as the radius of zero magnetic flux at middle cross section in simulation results from MPF-2D. From our calculation, the separatrix radius was 5 cm at $t = 1$ μs (here $t = 0$ denotes the trigger time of θ-pinch bank), and decreased to 1.36 cm at $t = 2.8$ μs because of the large magnetic pressure caused by θ-pinch coil. At the time of peak compression, the pressures inside and outside of the separatrix were balanced at radial direction. From Fig. 16(a), the calculated separatrix radius agrees well with the experimental data during the compression process and the calculated FRC target length is 39 cm in axial direction which is approximate to the experimental result of 34 cm. The target relaxes radially after peak compression and then the separatrix radius continuously oscillates due to the vibration of the θ-pinch field. During the relaxing process the difference between simulation and experiments increases. Fig. 16(b) shows the end-on images with the MPF-2D calculated results during plasma compression. The plasma temperature (electron temperature from MPF-2D is adopted here) at the middle cross section is distributed as varying color in simulations and presented by the self-luminance in images. The comparison of the end-on images confirms the processes of the FRC formation.

With the working gas H_2 of 8 Pa and the charging voltage of the mirror, bias, ionization and θ-pinch banks at 5 kV, 5 kV, 55 kV and ±30 kV (corresponding field values are 0.9 T, 0.2 T, 0.2 kV/cm and 1.7 T) respectively, the experiment data were plotted in Fig. 17. The waveform of magnetic field (black) and electron areal density from laser interferometer (red) are shown in Fig. 17(a) and the separatrix radii calculated by Formula (1) from the magnetic and flux probes array data are shown in Fig. 17(b). Fig. 17(c) shows the average plasma densities calculated by the formula

$$n_{\mathrm{m}} = \frac{n_0 \cdot x_{\mathrm{t}}^2}{\langle\beta\rangle x_{\mathrm{s}}^2 Z_{\mathrm{s}}}, \tag{2}$$

where n_0 is the density of neutral gas; $x_{\mathrm{t}} = r_{\mathrm{t}}/r_{\mathrm{c}}$ denotes the radius ratio of the tube and the θ-pinch coil; $\langle\beta\rangle = 1 - x_{\mathrm{s}}^2/2$ is the ratio of plasma thermal pressure and outer magnetic pressure; $x_{\mathrm{s}} = r_{\mathrm{s}}/r_{\mathrm{c}}$ is the relative radius of separatrix; r_{s} is the radius of separatrix; $Z_{\mathrm{s}} = l_{\mathrm{s}}/l_{\mathrm{c}}$ is the relative length of plasma target, where l_{s} is the length of target and l_{c} is the length of θ-pinch coil. Fig. 17(d) shows the average plasma equilibrium temperatures (assuming the ion temperature equals to the electron's) given by the Formula (3) derived from the ideal gas equation of state

$$\langle T\rangle = \frac{P_{\mathrm{B}}}{n_{\mathrm{m}} \cdot k}, \tag{3}$$

where $P_{\mathrm{B}} = B_{\mathrm{p}}^2/2\mu_0$ is the magnetic pressure, $\mu_0 = 4\pi \times 10^{-7}$ N/A^2 is the vacuum permeability, $k = 1.38 \times 10^{-23}$ J·K^{-1} is the Boltzmann constant. At $t = 572.4$ μs, the magnetic field of 1.7 T from B probes array, the separatrix radius of 4 cm from the magnetic and flux probes array, the electron areal density of 2.8×10^{17} cm^{-2} from single-chord laser interferometer, the average plasma density of 3.25×10^{16} cm^{-3} from Formula (2) and the average plasma equilibrium temperature of 212 eV from Formula (3) have been achieved in this shot. Assumed that there's no plasma outside of the separatrix, based on the measured radius of the separatrix and the electron areal density, the average electron density can be calculated to be

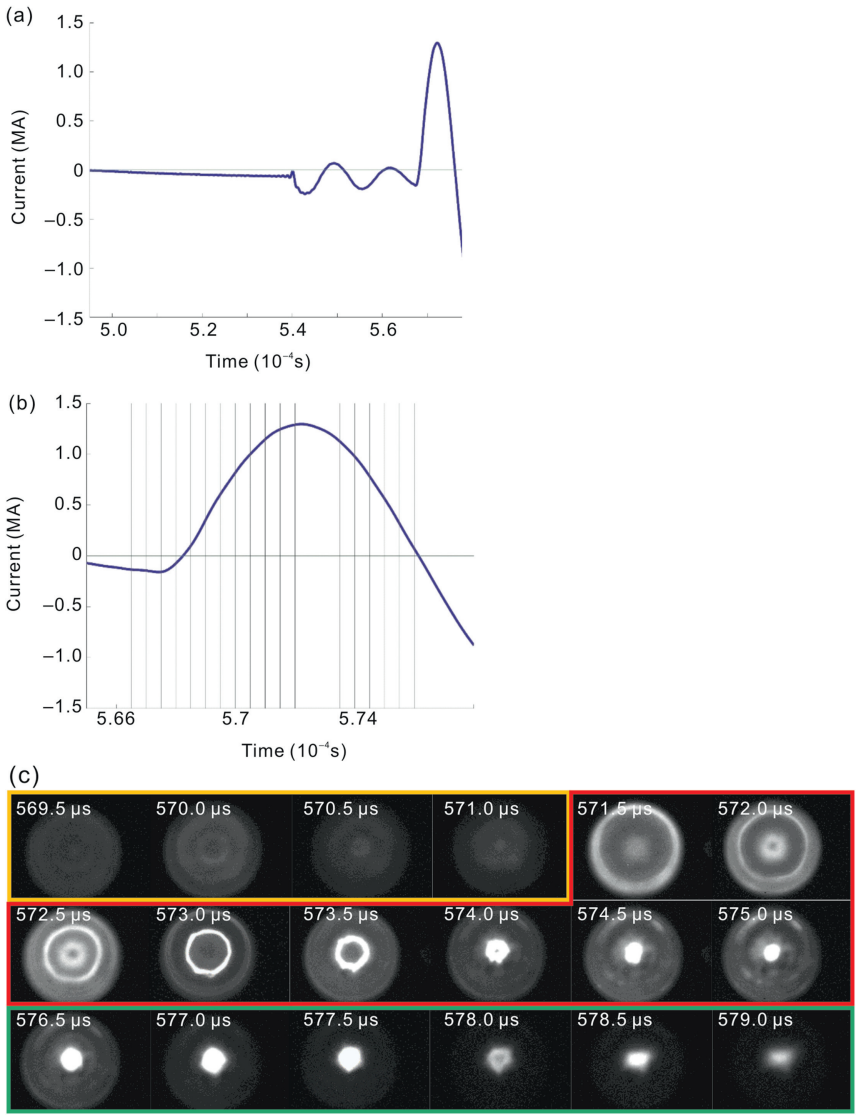

Fig. 15. Processes of FRC formation. (a) Current/magnetic field waveform; (b) Time of the images; (c) Images from the end-on camera with the exposure time of 10 ns.

3.5×10^{16} cm^{-3} at $t = 572.4$ μs, which agrees with that from the semi-empirical Formula (2).

5. Summary and future work

Yingguang-I is a multi-bank program-discharging pulsed power device to study the formation, confinement and instability of the high temperature and high density FRC plasma injector for MTF. The peak current/magnetic field of 110 kA/0.3 T, 10 kA/1.2 T and 1.7 MA/3.4 T have been achieved in the bias, mirror and θ-pinch circuit with the quarter cycle of 80 μs, 700 μs and 3.8 μs respectively and the device can operate repetitively. Recent works on Yingguang-I device have been focused on the gas ionization and the FRC formation. From the experimental results, we conclude that the bias magnetic field suppresses highly the gas ionization and we have obtained the limit of the bias field at a set-up ionization field. By the one-chord laser interferometer we can only obtain the electron chord-averaged density. To better evaluate the ionization efficiency, a multi-chord interferometer is being constructed to resolve the spatial–temporal evolution of plasma density. From the magnetic probes, flux probes, end-on high speed camera and the laser interferometer, the formation of FRC has been confirmed with the density, temperature and separatrix radius of about 10^{16} cm^{-3}, 200 eV, and 4 cm respectively. The experimental results agree with those from simulation by MPF-2D code. Due to the reversed field attenuation, quickly without the crowbar switch, the lifetime of FRC is only 3 μs, which approximately equals to the half pulse width of the reversed field. We have conducted the calculation to improve the device with crowbar switches which would be connected to the θ-pinch coils in parallel. With the aid of the crowbar switch, the half pulse width of the reversed field can be extended to more than 50 μs while the plasma lifetime is defined by the instabilities, the particles and energy transport, not by the half pulse width of the reversed field. The test is

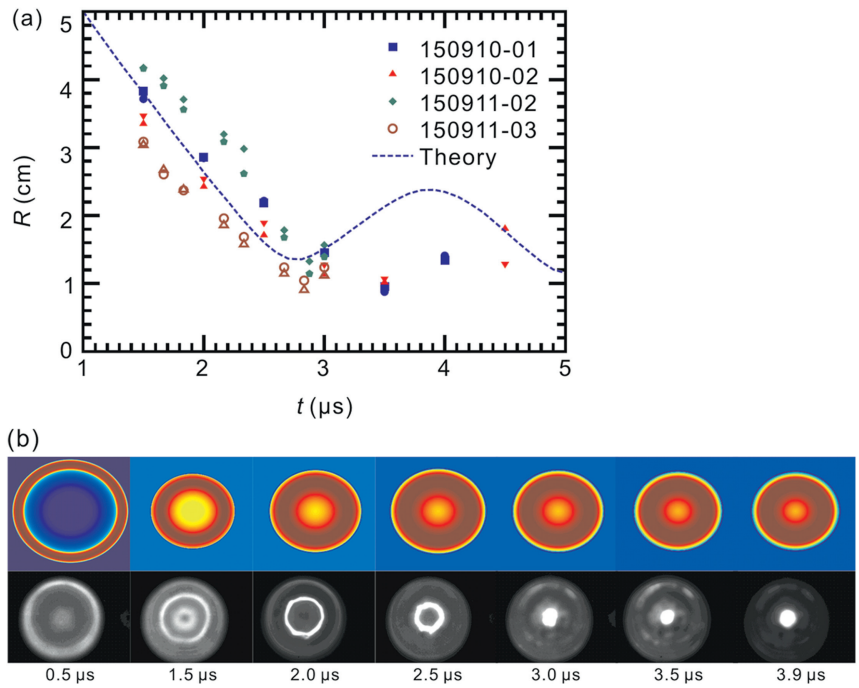

Fig. 16. Separatrix radii from the 2D-MHD and the experiments. (a) Evolution of separatrix calculated from MPF-2D compared to the experimental data. Blue square refers to shot 150910-01; red solid up and down triangle refers to shot 150910-02; green diamond refers to shot 150911-02; brown open circle and triangle refer to shot 150911-03. (b) End-on images during plasma compression – the results from 2D-MHD simulation (top) and the high-speed camera (bottom). The time of 0.5 μs refers to the time of 568.5 μs in Fig. 15(c).

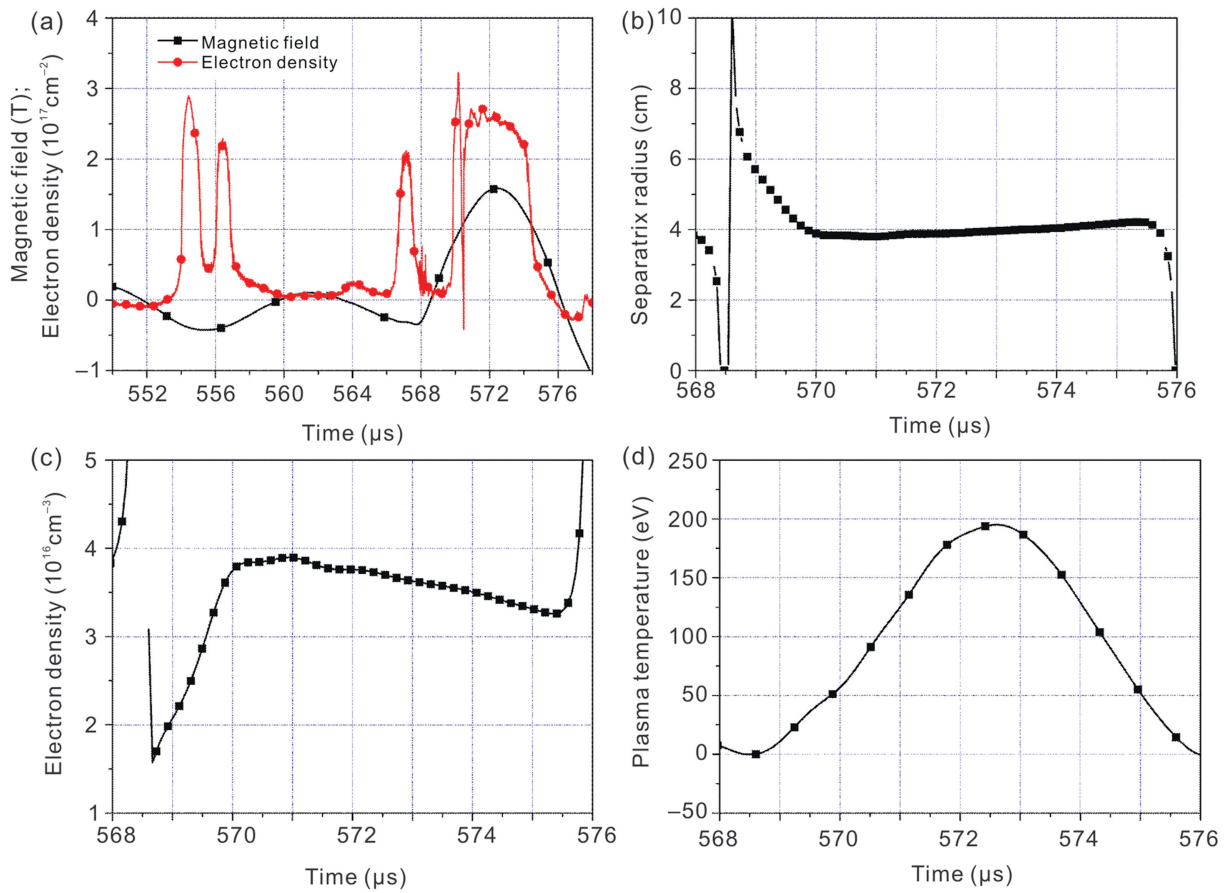

Fig. 17. Experimental results with H_2 of 8 Pa.

ongoing. On the Yingguang-I device the verification of the collision-merging approach to form a longer lifetime and more controllable FRC target is also in plan.

Acknowledgements

This work is supported by the National Natural Science Foundation of China (Grant Nos. 11375163, 11605182, 11605183), the Development Foundation of China Academy of Engineering Physics (Grant No. 2011B0402009) and the Science Challenge Project No. 2016212A505.

References

[1] H. Kishimoto, S. Ishida, M. Kikuchi, H. Ninomiya, Advanced tokamak research on JT-60, Nucl. Fusion 45 (2005) 986.
[2] O.A. Hurricane, D.A. Callahan, D.T. Casey, P.M. Celliers, C. Cerjan, et al., Fuel gain exceeding unity in an inertially confined fusion implosion, Nature 506 (2014) 343−348.
[3] I.R. Lindemuth, R.E. Reinovsky, R.E. Chrien, J.M. Christian, C.A. Ekdahl, et al., Target plasma formation for magnetic compression/ magnetized target fusion, Phys. Rev. Lett. 75 (1995) 1953.
[4] T.P. Intrator, J.Y. Park, J.H. Degnan, I. Furno, C. Grabowski, et al., A high-density field reversed configuration plasma for magnetized target fusion, IEEE Trans. Plasma Sci. 32 (2004) 152−160.
[5] L.C. Steinhauer, Review of field-reversed configurations, Phys. Plasmas 18 (2011) 070501.
[6] M. Tuszewski, Field reversed configurations, Nucl. Fusion 28 (1988) 2033.
[7] J.M. Finn, R.N. Sudan, Field-reversed configurations with a component of energetic particles, Nucl. Fusion 22 (1982) 1443.
[8] W.T. Armstrong, R.K. Linford, J. Lipson, D.A. Platts, E.G. Sherwood, Field-reversed experiments (FRX) on compact toroids, Phys. Fluids 24 (1981) 2068.
[9] R.E. Siemon, W.T. Armstrong, R.R. Bartsch, Experimental studies of field-reversed-configuration (FRC) confinement in FRX-C, in: Plasma Physics and Controlled Nuclear Fusion Research, Vol. 2, IAEA, Vienna, 1983, p. 283.
[10] T. Intrator, S.Y. Zhang, J.H. Degnan, I. Furno, C. Grabowski, et al., A high density field reversed configuration (FRC) target for magnetized target fusion: first internal profile measurements of a high density FRC, Phys. Plasmas 11 (2004) 2580.
[11] J.H. Degnan, D.J. Amdahl, M. Domonkos, et al., Recent Magneto-Inertial Fusion Experiments on FRCHX, LA-UR-13-20426.
[12] G.A. Wurden, S.C. Hsu, T.P. Intrator, et al., Magneto-inertial fusion, J. Fusion Energy 35 (2016) 69−77.
[13] S. Kumashiro, T. Takahashi, M. Ooi, T.S. Takahashi, S. Shimamura, et al., Sources of fluctuating field on field-reversed configuration plasma, J. Phys. Soc. Jpn. 62 (1993) 1539.
[14] Y. Ono, A. Morita, M. Katsurai, M. Yamada, Experimental investigation of three-dimensional magnetic reconnection by use of two colliding spheromaks, Phys. Fluid B 5 (1993) 3691.
[15] E. Kawamori, Y. Ono, Effect of Ion Skin Depth on Relaxation of Merging Spheromaks to a Field-Reversed Configuration, Phys. Rev. Lett. 95 (2005) 085003.
[16] M. Yamada, H. Ji, S. Hsu, T. Carter, R. Kulsrud, et al., Study of driven magnetic reconnection in a laboratory plasma, Phys. Plasmas 4 (1997) 1936.
[17] M.W. Binderbauer, H.Y. Guo, M. Tuszewski, et al., Dynamic formation of a hot field reversed configuration with improved confinement by supersonic merging of two colliding high-β compact toroids, Phys. Rev. Lett. 105 (2010) 045003.
[18] M. Tuszewski, A. Smirnov, M.C. Thompson, et al., Field Reversed Configuration confinement enhancement through edge biasing and neutral beam injection, PRL 108 (2012) 255008.
[19] Y. Razin, A direct fusion drive for rocket propulsion, Acta Astronaut. 105 (1) (December 2014) 145−155.
[20] A.L. Hoffman, H.Y. Guo, J.T. Slough, S.J. Tobin, L.S. Schrank, et al., The TCS rotating magnetic field FRC current-drive experiment, Fusion Sci. Technol. 41 (2002) 92.
[21] H.Y. Guo, A.L. Hoffman, R.D. Milroy, Rotating magnetic field current drive of high-temperature field reversed configurations with high ζ scaling, Phys. Plasmas 14 (2007) 112502.
[22] T. Munsat, C.L. Ellison, A. Light, J. Nuger, W. Willcockson, et al., The colorado FRC experiment, J. Fusion Energy 27 (2008) 82.
[23] W.S. Harris, E. Trask, T. Roche, E.P. Garate, W.W. Heidbrink, et al., Ion flow measurements and plasma current analysis in the Irvine Field Reversed Configuration, Phys. Plasmas 16 (2009) 112509.
[24] Qi-Zhi Sun, Dong-Fan Fang, Wei Liu, Wei-Dong Qing, Yue-Song Jia, et al., Physical design of the Yingguang-I device, Acta Phys. Sin. 62 (2013) 78407.
[25] J.M. Taccetti, T.P. Intrator, G.A. Wurden, S.Y. Zhang, R. Aragonez, et al., FRX-L: a field-reversed configuration plasma injector for magnetized target fusion, Rev. Sci. Instrum. 74 (2003) 4314−4323.
[26] S.A. Cohen, B. Berlinger, C. Brunkhorst, A. Brooks, N. Ferraro, et al., Formation of collisionless high-β plasmas by odd-parity rotating magnetic fields, Phys. Rev. Lett. 98 (2007) 145002.
[27] M. Laberge, An acoustically driven magnetized target fusion reactor, J. Fusion Energy 27 (2008) 65−68.
[28] G.A. Wurden, K.F. Schoenberg, R.E. Siemon, M. Tuszewski, F.J. Wysocki, et al., Magnetized target fusion: a burning FRC plasma in an imploded metal can, J. Plasma Fusion Res. 2 (1999) 238−241.
[29] M. Laberge, Experimental results for an acoustic driver for MTF, J. Fusion Energy 28 (2009) 179−182.
[30] S.C. Hsu, T.J. Awe, S. Brockington, A. Case, J.T. Cassibry, et al., Spherically imploding plasma liners as a standoff driver for magneto-inertial fusion, IEEE Trans. Plasma Sci. 40 (2012) 1287−1298.
[31] C. Grabowski, J.H. Degnan, D.J. Amdahl, M. Domonkos, E.L. Ruden, et al., Addressing short trapped-flux lifetime in high-density field-reversed configuration plasmas in FRCHX, IEEE Trans. Plasma Sci. 42 (2014) 1179−1188.
[32] H.Y. Guo, M.W. Binderbauer, D. Barnes, S. Putvinski, N. Rostoker, et al., Formation of a long-lived hot field reversed configuration by dynamically merging two colliding high-β compact toroidsa, Phys. Plasmas 18 (2011) 056110.
[33] S.A. Slutz, M.C. Herrmann, R.A. Vesey, A.B. Sefkow, D.B. Sinars, et al., Pulsed-power-driven cylindrical liner implosions of laser preheated fuel magnetized with an axial fielda, Phys. Plasmas 17 (2010) 056303.
[34] M. Laberge, S. Howard, D. Richardson, A. Froese, V. Suponitsky, et al., Acoustically driven magnetized target fusion, in: IEEE 25th Symposium on Fusion Engineering, vol 42, 2013.
[35] D.F. Fang, Q.Z. Sun, X.M. Zhao, Y.S. Jia, Design of a fully-fiber multi-chord interferometer and a new phase-shift demodulation method for field-reversed configuration, Rev. Sci. Instrum. 85 (2014) 053510.
[36] L.L. Li, H. Zhang, X.J. Yang, Two-dimensional magneto-hydrodynamic description of field reversed configuration, Acta Phys. Sin. 63 (2014) 165202.
[37] L.L. Li, H. Zhang, X.J. Yang, Optimization of Field Reversed Configuration for "Ying-Guang 1", High Power Laser and Particle Beams 27 045006.
[38] L.L. Li, H. Zhang, X.J. Yang, Translation process of field reversed configuration, Acta Phys. Sin. 64 (2015) 125202.